# Accurate representation of poroelastic thin layers as interface conditions

Marco Favino[0000−0002−1253−9164] and
Nicolás D. Barbosa[0000−0001−5243−9080] and
Rolf Krause[0000−0001−5408−5271] and
Klaus Holliger[0000−0002−2584−8177]

**Abstract** The evaluation of propagation of seismic waves in fractured porous media is a critical endeavor in Earth Sciences and, hence, assessing attenuation and velocity dispersion through numerical simulations of Biot's equations of poroelasticity in the frequency-space is of large significance. The generation of meshes for fractured media using equi-dimensional representations, where fractures have a thin but finite apertures, remains one of the primary limitations in simulating seismic wave propagation in fractured media. Therefore, numerical methods based on hybrid-dimensional models, featuring the downscaling of fractures to lower dimensions as well as the use of suitable interface conditions, is fundamental for enabling the simulation of realistic fractured media. Drawing inspiration from the pertinent literature in Darcy flow simulations, interface conditions are usually based on the assumption of linear distributions of relevant fields across fractures. However, in the context of poroelasticity, linear approximations may not capture the full complexity of the solution of Biot's equations, and require the introduction of correction terms to enhance the accuracy of numerical simulations. This work explores the nature and importance of interface conditions. In the context outlined above, it presents a formal derivation of corrected interface conditions from the analytical solution of Biot's equations, and compares numerical results obtained with a linear approximation against the ones obtained with the corrected interface conditions. Numerical experiments conducted for a range of material properties emphasize the necessity of incorporating the correction terms for accurate simulations.

Marco Favino
Name, Address of Institute, e-mail: marco.favino@unidistance.ch

Nicolás D. Barbosa
SINTEF Industri, Trondheim, Norway. e-mail: nicolas.barbosa@sintef.no

Rolf Krause
Faculty of Mathematics and Computer Science, Unidistance Suisse, Switzerland. e-mail: rolf.krause@fernuni.ch

Klaus Holliger
Institute of Earth Sciences, University of Lausanne, Switzerland. e-mail: klaus.holliger@unil.ch

# 1 Introduction

The exploration of seismic wave attenuation and velocity dispersion in fractured media through numerical simulations is pivotal for understanding and constraining the mechanical and hydraulic properties of heterogeneous porous rocks [14, 13, 9, 10]. This knowledge is essential for a wide range of pertinent applications throughout the Earth, environmental, and engineering sciences, such as, for example energy production, hydrocarbon exploration, nuclear waste disposal, and $CO_2$ storage.

From a mathematical perspective, assessing attenuation and velocity dispersion involves computing post-processed quantities based on stress and strain distributions in poroelastic fractured media [6]. The primary challenge arises from solving Biot's equations of poroelasticity in the space-frequency domain in heterogeneous media [14, 13, 6], containing intricate networks of thin high-contrast fractures. This computational task is crucial for gaining insights into the behavior of seismic waves in complex geological formations.

Numerical simulations of fractured media present significant challenges. Firstly, generating meshes for full *equi-dimensional* models, where fractures are represented as heterogeneities of the same geometric dimension as the background, is practically unfeasible for realistic fracture networks [1, 3]. Equi-dimensional models typically result in meshes with elongated elements [7], compromising numerical solution accuracy. Secondly, analytical solutions for problems involving heterogeneous material properties often exhibit low regularity, thus, impacting the convergence of employed numerical methods [8].

To address these challenges, *hybrid-dimensional* models have been developed [11, 7, 2]. These models downscale fractures to lower-dimensional objects, thus, simplifying mesh generation and introducing tailored interface conditions to accurately capture cross-fracture physics. Embraced in Darcy flow simulations, hybrid-dimensional models are based on the assumption of linear distributions of fluid velocity and pressure across fractures. For Biot's equations in the space-time domain, hybrid-dimensional models have been presented in [5, 4].

However, for Biot's equations in the space-frequency domain, the linear approximation does not allow to capture the complexity of the solution of Biot's equations in thin layers. In [12], corrected interface conditions have been derived by integrating the governing equations over a poroelastic thin layer.

Here, we present a formal derivation of both the linear and corrected interface conditions, with the latter obtained from an analytical solution to Biot's equations. We then conduct a numerical comparison of the application of these two sets of interface conditions across different permeabilities of fractures. Our results demonstrate the necessity of employing the corrected interface conditions to accurately reproduce the behavior of seismic waves in fractured porous media.

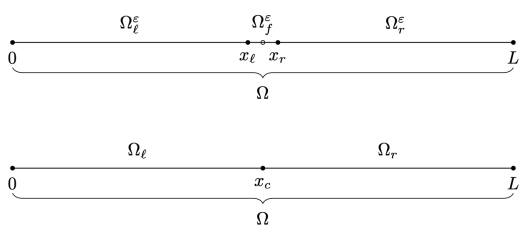


(a) The domain $\Omega$ with the fracture $\Omega_f^\varepsilon$ (top). The subdomains $\Omega_\ell$ and $\Omega_r$ separated by the fracture considered as an interface (bottom).

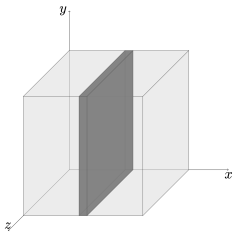


(b) Cartesian coordinate system.

**Fig. 1** Geometry of the considered fractured media.

## 2 Equi-dimensional model

We consider the domain $\Omega$ as the interval $(0, L) \subset \mathbb{R}$, representing coordinates along an axis orthogonal to a fracture plane in three-dimensional media, (Figure 1). Assuming transversely isotropic media, Biot's one-dimensional equations in the space-frequency domain describe the hydro-mechanical coupling in a deformable porous media along an axis orthogonal to the fracture plane. The equations read as follows:

$$-\sigma' = 0 \qquad (1) \qquad\qquad \frac{w'}{j\omega} = -\alpha u' - mp \qquad (3)$$

$$\sigma = hu' - \alpha p \qquad (2) \qquad\qquad w = -kp', \qquad (4)$$

where the displacement $u$ ([Length]), the relative fluid-solid velocity $w$ ([Length] $\times$ [Time]$^{-1}$), the total stress $\sigma$ ([Pressure]), and the pressure $p$ ([Pressure]) are complex functions defined from $\Omega$ into $\mathbb{C}$. The material properties and their dimensions are: $h$ the bulk modulus (Pressure), $\alpha$ the Biot-Willis coefficient (dimensionless), $m$ the storativity ([Pressure]$^{-1}$), and $k$ the fluid mobility ([Length]$^2$ $\times$ [Pressure]$^{-1}$ $\times$ [Time]$^{-1}$). Non-bold lowercase letters are employed to stress that quantities at hand are scalar, and $'$ denotes the derivative with respect to $x$ co-ordinate.

From a mathematical standpoint, Eqs. (1) and (3) are balance equations with associated fluxes $\sigma$ and $w$. Eqs. (2) and (4) are closure relations between fluxes and primal variables $u$ and $p$. Hence, replacing the definitions of the fluxes into the balance equations leads to the following system:

$$-(hu' - \alpha p)' = 0 \qquad (5) \qquad\qquad -\alpha u' - mp + \left(\frac{k}{j\omega} p'\right)' = 0. \qquad (6)$$

The fracture domain $\Omega_f^\varepsilon = (x_\ell, x_r)$ is a subdomain of $\Omega$, whose center is $x_c$ and aperture is $\varepsilon$. The background domain instead is defined as $\Omega_b^\varepsilon = \Omega \setminus \Omega_f^\varepsilon$. We also assume that $\Omega_f^\varepsilon$ separates $\Omega_b^\varepsilon$ into two subdomains $\Omega_\ell^\varepsilon = (0, x_\ell)$ and $\Omega_r^\varepsilon = (x_r, L)$ (upper portion of Figure 1a). We assume that the material properties may assume

different values in the background and in the fracture domains. We denote their values using the subscripts $_b$ and $_f$, e.g., $k_b$ and $k_f$.

If we denote with the subscript $_i$ the restriction of a variable over the the domain $\Omega_i^\varepsilon$ (e.g., $p_b = p|_{\Omega_b^\varepsilon}$), we can restrict Biot's equation to such a domain coupled with the following transmission conditions:

$$v_b(x_i) = v_f(x_i) \tag{7}$$

with $i \in \{\ell, r\}$ and $v \in \{u, \sigma, w, p\}$.

## 3 Linear interface conditions

The thin dimension of the aperture points to replace the equations pertaining to the fracture domain with suitable interface conditions. The basic idea is to define the governing equations over two domains $\Omega_\ell = (0, x_c)$ and $\Omega_r = (x_c, L)$, assuming that the variables may be discontinuous at $x_c$. We employ the standard notation used for interface problems, where the jump of a function $v$ at $x_c$ is denoted by $[v] = v_r(x_c) - v_\ell(x_c)$ and the mean value by $\{v\} = \frac{v_r(x_c)+v_\ell(x_c)}{2}$.

Following the presentation of [11], the steps in order to obtain the interface conditions are the following. First, integrate the equations over the fracture domain $\Omega_f^\varepsilon$. The integrals of derived quantities can be directly evaluated, while the integrals of non-derived quantities are computed by means of a trapezoidal quadrature rule. This latter is the only approximation employed in the derivation of the interface conditions. In this way, we obtain algebraic expressions for the displacement, stress, pressure and the velocity in the fracture at $x_\ell$ and $x_r$. Second, we replace the transmission conditions (7) in the obtained relations to write these latter with respect to the variables in the background. Third, we take the limits $x_i \to x_c$ for $i \in \{\ell, r\}$. Applying these steps, we obtain the following:

**Linear interface equations**

$$[\sigma] = 0 \tag{8}$$

$$\{\sigma\} = \frac{h}{\varepsilon}[u] - \alpha\{p\} \tag{9}$$

$$\frac{[w]}{j\omega} = -\alpha[i] - \varepsilon m\{p\} \tag{10}$$

$$\{w\} = -\frac{k}{\varepsilon}[p], \tag{11}$$

A valuable insight arises from comparing the Biot's equations model with the arising interface conditions. This comparison reveals a straightforward rule for transitioning from equi-dimensional models to interface conditions: replace function derivatives with jumps and function evaluations with mean values.

# 4 Corrected interface conditions

In the derivation of the linear interface conditions, we utilized a trapezoidal quadrature rule to approximate the integral of $w$ and other unknown quantities. This methodology is equivalent to assuming a linear distribution of the relevant unknowns in Biot's equations across the fracture, e.g., assuming that $w_f^\varepsilon(x)$ can be approximated as

$$w_f^\varepsilon(x) \approx w_f(x_\ell)\phi_\ell(x) + w_f(x_r)\phi_r(x), \tag{12}$$

where $\phi_\ell(x) = \frac{x_r - x}{\epsilon}$ and $\phi_r(x) = \frac{x - x_\ell}{\epsilon}$. In the following subsection, we derive an exact expression for $w_f^\varepsilon(x)$ and the other unknwons in the fracture domain employing the analytical solutions to reaction-diffusion problems. This exact expression is employed to derive the corrected interface conditions.

## 4.1 Analytical solutions to reaction-diffusion problems

By means of algebraic manipulations the coupled system of equations (5) and (6) can be written as two non-coupled reaction-diffusion equations in $\Omega_f^\epsilon$

$$-u'' + \sigma u = C\phi_\ell + D\phi_r, \tag{13} \qquad -p'' + \sigma p = E, \tag{14}$$

where $C$, $D$, and $E$ are constant values and $\sigma = j\omega\left(\frac{m}{k} + \frac{\alpha^2}{kh}\right) = \delta^2$, whose physical dimension is $[\text{Length}]^{-2}$. The corresponding real component of $\delta$ is the inverse of the diffusion length. Solutions to (14) and (14) can be explicitly computed and read

$$u(x) = u_\ell\varphi_\ell(x) + u_r\varphi_r(x) + F\psi_\ell(x) + G\psi_r(x), \tag{15}$$

$$p(x) = p_\ell\varphi_\ell(x) + p_r\varphi_r(x) + H\psi_\ell(x) \tag{16}$$

where $\varphi_\ell = \frac{\sinh(\delta(x_r - x))}{\sinh(\delta\varepsilon)}$, $\varphi_r = \frac{\sinh(\delta(x - x_\ell))}{\sinh(\delta\varepsilon)}$, $\psi_\ell = \phi_\ell - \varphi_\ell$, $\psi_r = \phi_r - \varphi_r$, and $\psi_c = 1 - \varphi_\ell - \varphi_r$. The constants $F$, $G$, and $H$ are to be determined.

## 4.2 Derivation of analytical interface conditions

Since $u \in \text{span}(\varphi_\ell, \varphi_r, \psi_\ell, \psi_r)$ and $p \in \text{span}(\varphi_\ell, \varphi_r, \psi_c)$, their exact analytical expression can be computed in $\Omega_f^\epsilon$. Hence, performing the same procedure of the Section 3 with the only difference that the integrals that have been previously approximated with a trapezoidal rule are now exactly evaluated. This procedure leads to the following:

**Corrected interface equations**

$$[\sigma] = 0 \tag{17}$$

$$\{\sigma\} = \Delta\left(\frac{h}{\varepsilon}[u] - \alpha\Pi\{p\}\right) \tag{18}$$

$$\frac{[w]}{j\omega} = -\Delta\Pi\left(\alpha[u] + \varepsilon m\{p\}\right) \tag{19}$$

$$\{w\} = -\frac{1}{\Pi}\frac{k}{\varepsilon}[p]. \tag{20}$$

The derived interface equations have a structure similar to the ones in (8), (9), (10), and (11) but they feature the two correction terms $\Pi = \frac{\tanh(\delta\varepsilon/2)}{\delta\varepsilon/2}$ and $\Delta = \frac{mh+\alpha^2}{mh+\Pi\alpha^2}$.

## 5 Numerical results

In this section, we examine the attenuation and velocity dispersion characteristics, as well as the displacement distributions at some relevant frequencies, obtained from the two hybrid-dimensional models comparing them with the results derived from the equi-dimensional model, which serves as our reference benchmark. The domain size is set at $L = 200$mm, with the fracture center positioned at $x_c = 100$mm, and the fracture thickness defined as $\varepsilon = 2$mm.

We consider two distinct sets of material properties: one featuring a conductive fracture and another featuring blocking fractures. The material properties for the conductive case are obtained from [6]. For the blocking case, we modified the fluid mobility in the fracture to $k_f = 10^{-5}\text{mm}^2\times\text{kPa}^{-1}$. Regarding the boundary conditions, we prescribe $u(0) = 0$, $u(L) = -10^{-3}$mm, and $w(0) = w(L) = 0$.

### 5.1 Conductive case

The resulting attenuation and velocity dispersion curves are shown in Figures 2a and 2b, respectively. Both the linear and the corrected interface conditions provide similar results, which are also consistent with the reference solution. From the plots of the correction parameters $\Delta$ and $\Pi$, reported in Figures 2c and 2d, respectively, we observe that they are unitary up to a frequency of $10^4$ Hz, meaning that up to this frequency the two sets of interface conditions are similar. At larger frequencies, the two correction parameters $\Pi$ and $\Delta$ present significant deviation from the real unit. However, their product (not reported) remains in the range of the real unit, suggesting a compensating effect between the two correction parameters and explaining the correct evaluation of the attenuation and velocity dispersion curves.

The hypothesis of a linear approximation is further substantiated graphically by the distributions of the solutions depicted in Figures from 3a to 3d. Both the displacement and the pressure (though not reported) exhibit a linear trend within the fracture. In the zoomed-in plots of Figures 3a and 3b, we observe that at low frequencies ($\nu = 10^0$ Hz), both interface models precisely replicate the displacement drop within the fracture. However, subtle differences emerge in the real component of the displacement at $\nu = 10^5$ Hz (Figure 3c) between the equi-dimensional and the two interface models, although the latter two exhibit no discernible distinctions between them. In the distribution of the imaginary component of the displacement at $\nu = 10^5$ Hz (Figure 3d), two oscillations are noticeable in the equi-dimensional model precisely at the fracture-background junctions, specifically at $x_\ell$ and $x_r$. These oscillations are similarly replicated by the two interface models, exhibiting the correct amplitude, albeit being shifted closer to the interface at $x_c$.

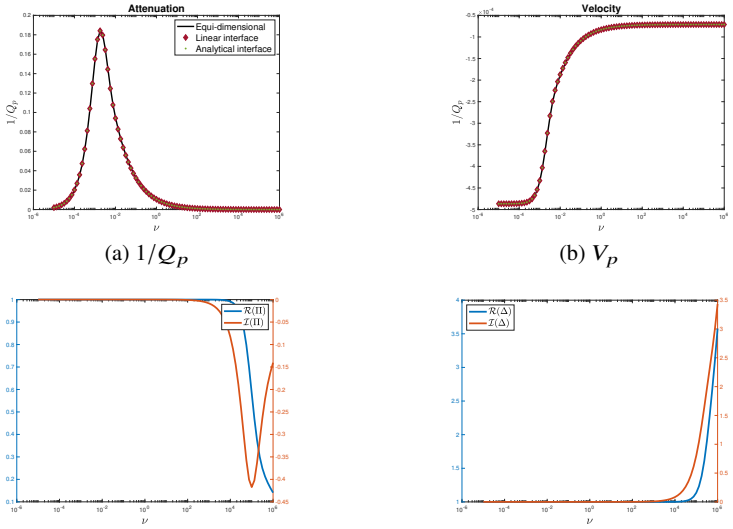


(a) $1/Q_p$ (b) $V_p$

(c) $\Pi$ (d) $\Delta$

**Fig. 2** Conductive case: attenuation (a), velocity (b), correction parameter $\Pi$ (c), correction parameter $\Delta$ (d).

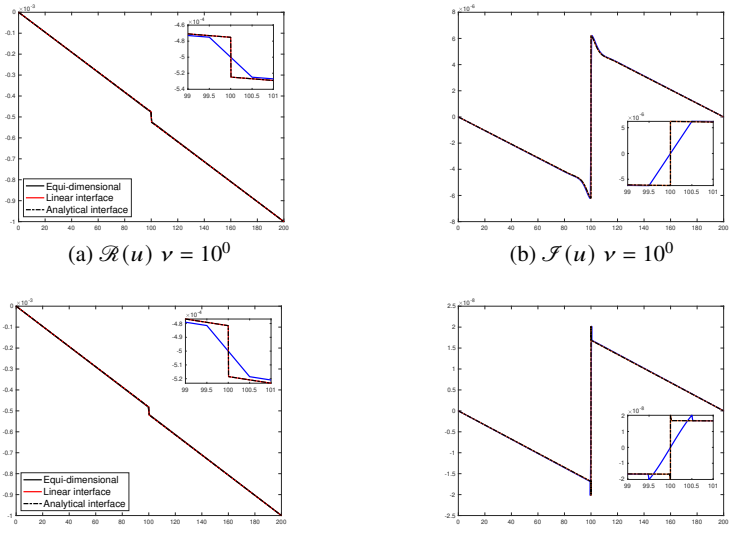


(a) $\mathscr{R}(u)$ $\nu = 10^0$ (b) $\mathscr{I}(u)$ $\nu = 10^0$

(c) $\mathscr{R}(u)$ $\nu = 10^5$ (d) $\mathscr{I}(u)$ $\nu = 10^5$

**Fig. 3** Conductive case: real (a) and imaginary (b) displacement at $\nu = 10^0$, real (c) and imaginary (d) displacement at $\nu = 10^5$.

## 5.2 Blocking case

In the blocking case, significant differences arise between the results obtained with linear interface model and the corrected one. Figures 4a and 4b show that the attenuation and velocity dispersion curves calculated with the corrected interface conditions perfectly agree with those from the reference equi-dimensional model. Conversely, the linear interface conditions lead to a peak frequency shifted toward higher values, higher attenuation, and underestimated velocity dispersion. Notably, both approaches accurately reproduce the curves at extremely low and high frequencies.

Figures 4c and 4d reveal a key distinction from the conductive case. Here, the two correction parameters deviate most significantly from unity in the central frequencies, suggesting their fundamental role in this regime. At higher frequencies, the correction parameter $\Pi$ approaches zero, implying that mechanical deformations and fluid flow become uncoupled.

The real and imaginary components of the displacement at $\nu = 10^{-2}$ Hz are presented in Figures 5a and 5b, respectively. Figures 5c and 5d show the real and imaginary components of the pressure at the same frequency. We observe that the curves obtained with the analytical interface conditions generally align better with those from the equi-dimensional model in the background domain far from the fracture. However, significant discrepancies occur near the fracture, where the linear interface model apparently is closer to capture the internal fracture characteristics.

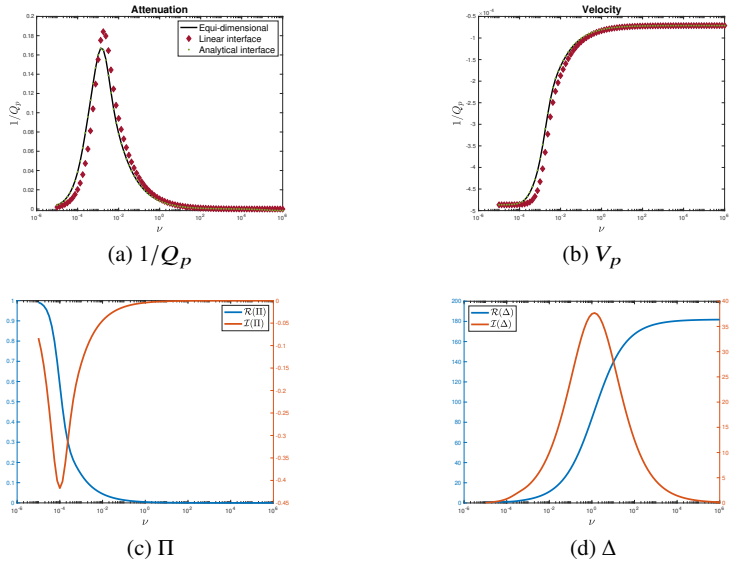


(a) $1/Q_p$ (b) $V_p$

(c) $\Pi$ (d) $\Delta$

**Fig. 4** Blocking case: attenuation (a), velocity (b), correction parameter $\Pi$ (c), correction parameter $\Delta$ (d).

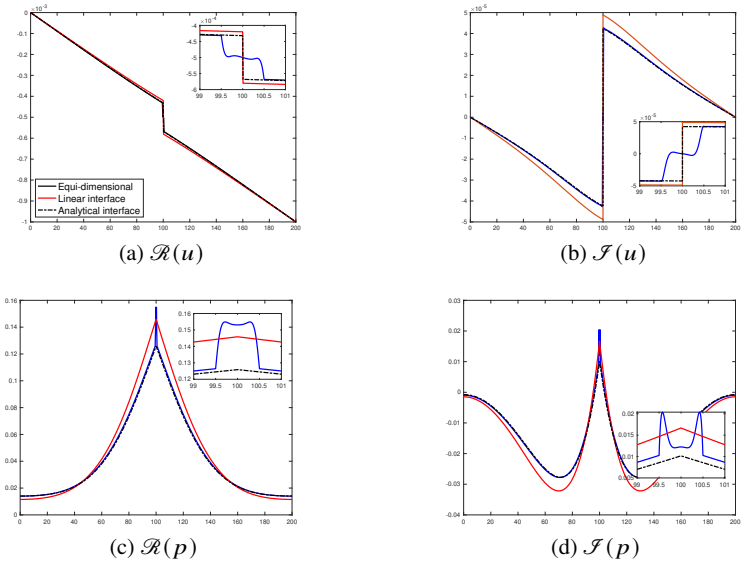


(a) $\mathscr{R}(u)$ (b) $\mathscr{I}(u)$

(c) $\mathscr{R}(p)$ (d) $\mathscr{I}(p)$

**Fig. 5** Blocking case: real (a) and imaginary (b) displacement at $\nu = 10^{-2}$, real (c) and imaginary (d) pressure at $\nu = 10^{-2}$.

## 6 Conclusions

We have presented two sets of interface conditions to downscale thin heterogeneities, specifically fractures, in the context of Biot's equations in the frequency-space domain. The first set assumes a linear distribution of the relevant fields in Biot's equations and leads to straightforward interface conditions. The second set is derived exploting the analytical solution of one-dimensional Biot's equations. These conditions resemble the structure of the linearly approximated ones, but incorporate correction terms dependent solely on material properties within the fractures.

Numerical evaluations of the attenuation and velocity dispersion of seismic waves in fractured media demonstrate that for both interface models yield identical outcomes conductive fractures. However, in the case of blocking fractures, the correction terms become pivotal for accurately reproducing the correct curves. A straightforward assessment of the correction terms can guide the need for their inclusion in equations. However, due to its simplicity, we recommend including the correction term in codes involving such downscaling, as failing to do so may lead to inaccurate evaluations.

In two- and three-dimensional settings, the extension of the interface conditions must account for stress components tangential to the fractures. The linear conditions can be readily derived by extending the methodology outlined in Section 3. While this process is relatively straightforward, it is essential to ascertain the range of material properties and frequencies for which they remain applicable, not only in compression tests as demonstrated, but also in shear tests. Conversely, deriving

corrected interface conditions is considerably more complex, as they rely on the analytical solution of Biot's equation, which is available only for simplified geometries. One possible approach to include them would be to omit the ones for components of the stress tangential to the fracture and utilize the presented conditions solely for the normal component. However, this introduces an approximation, necessitating a careful examination of its validity range.

## Acknowledgements

The contribution of Marco Favino is based on work supported by the Swiss National Science Foundation (SNSF) under Grant No. PZ00P2_180112. Rolf Krause would like to thank the Swiss National Science Foundation for their support through the project 200020E_186407 and the Deutsche Forschungsgemeinschaft (DFG) for their support in the SPP 1962. [186407].

## References

1. Antonietti, P.F., Formaggia, L., Scotti, A., Verani, M., Verzott, N.: Mimetic finite difference approximation of flows in fractured porous media. ESAIM: Mathematical Modelling and Numerical Analysis **50**(3), 809–832 (2016)
2. Berre, I., Boon, W.M., Flemisch, B., Fumagalli, A., Gläser, D., Keilegavlen, E., Scotti, A., Stefansson, I., Tatomir, A., Brenner, K., et al.: Verification benchmarks for single-phase flow in three-dimensional fractured porous media. Advances in Water Resources **147**, 103759 (2021)
3. Berre, I., Doster, F., Keilegavlen, E.: Flow in fractured porous media: A review of conceptual models and discretization approaches. Transport in Porous Media **130**(1), 215–236 (2019)
4. Boon, W.M., Nordbotten, J.M.: Mixed-dimensional poromechanical models of fractured porous media. Acta Mechanica **234**(3), 1121–1168 (2023)
5. Brezina, J., Stebel, J.: Mixed-dimensional model of poroelasticity (2022)
6. Favino, M., Hunziker, J., Caspari, E., Quintal, B., Holliger, K., Krause, R.: Fully-automated adaptive mesh refinement for media embedding complex heterogeneities: application to poroelastic fluid pressure diffusion. Computational Geosciences pp. 1–20 (2019)
7. Flemisch, B., Berre, I., Boon, W., Fumagalli, A., Schwenck, N., Scotti, A., Stefansson, I., Tatomir, A.: Benchmarks for single-phase flow in fractured porous media. Advances in Water Resources **111**, 239–258 (2018)
8. Grisvard, P.: Elliptic problems in nonsmooth domains. SIAM (2011)
9. Hunziker, J., Favino, M., Caspari, E., Quintal, B., Rubino, J.G., Krause, R., Holliger, K.: Seismic attenuation in realistic fracture networks. In: Poromechanics VI, pp. 1565–1572. Sixth Biot Conference on Poromechanics (2017)
10. Hunziker, J., Favino, M., Caspari, E., Quintal, B., Rubino, J.G., Krause, R., Holliger, K.: Seismic attenuation and stiffness modulus dispersion in porous rocks containing stochastic fracture networks. Journal of Geophysical Research: Solid Earth **123**(1), 125–143 (2018)
11. Martin, V., Jaffré, J., Roberts, J.E.: Modeling fractures and barriers as interfaces for flow in porous media. SIAM Journal on Scientific Computing **26**(5), 1667–1691 (2005)
12. Nakagawa, S., Schoenberg, M.A.: Poroelastic modeling of seismic boundary conditions across a fracture. The Journal of the Acoustical Society of America **122**(2), 831–847 (2007)
13. Rubino, J.G., Caspari, E., Müller, T.M., Milani, M., Barbosa, N.D., Holliger, K.: Numerical upscaling in 2-D heterogeneous poroelastic rocks: Anisotropic attenuation and dispersion of seismic waves. Journal of Geophysical Research: Solid Earth **121**, 6698–6721 (2016)
14. Rubino, J.G., Ravazzoli, C.L., Santos, J.E.: Equivalent viscoelastic solids for heterogeneous fluid-saturated porous rocks. Geophysics **74**, N1–N13 (2009)